Int. J. Electrochem. Sci., 7 **(2012)** 9909 - 9919

International Journal of
ELECTROCHEMICAL
SCIENCE
www.electrochemsci.org

Synthesis, Characterization and Electrocatalytic Activity of Bi- and Tri-metallic Pt-Based Anode Catalysts for Direct Ethanol Fuel Cells

C. D'Urso[1,*], *A. Bonesi*[2], *W. E. Triaca*[2], *A.M. Castro Luna*[2], *V. Baglio*[1], *A.S. Aricò*[1]

[1] CNR-ITAE, Via Salita S. Lucia sopra Contesse 5 - 98126 Messina, Italy
[2] INIFTA, Casilla de Correo 16, Succursal 4, (1900) La Plata Argentina
[*]E-mail: durso@itae.cnr.it

Received: 30 July 2012 / *Accepted:* 11 September 2012 / *Published:* 1 October 2012

Three Pt-based anode catalysts supported on Vulcan XC-72R (VC) were prepared by using a modified polyol process. These materials were characterized and tested by X-Ray Diffraction (XRD), X-Ray Fluorescence (XRF) and Transmission Electron Microscopy (TEM). XRD and TEM analysis indicated that especially the ternary anode catalysts consisted of uniform nanosized particles with sharp distribution. The Pt lattice parameter was smaller, in the ternary PtSnIr catalyst whereas it increased with the addition of Sn and Rh, in the corresponding binary and ternary catalysts. Cyclic voltammetry (CV) measurements showed that Sn, Ir and Rh may act as promoter of Pt enhancing ethanol electro-oxidation activity. It was found that the direct ethanol fuel cell (DEFC) performances were significantly improved with these modified anode catalysts. This effect on the DEFC performance is attributed to the so-called bi-tri-functional mechanism and to the electronic interaction between Pt and additives. The performance increased significantly with the temperature. However, it was also possible to observe some decay with time for all catalysts due to the formation of surface poisons, probably consisting in CO-like species. At 60 °C, the PtSnIr catalyst showed the best performance, as a result of a proper morphology and promoting effect.

Keywords: Direct ethanol fuel cells, ternary electrocatalysts, ethanol electro-oxidation, CO stripping.

1. INTRODUCTION

Low-temperature fuel cells fed directly with liquid fuels such as methanol and ethanol characterised by high energy density are gaining large interest especially for the huge potential market of fuel cells for portable and vehicle applications [1]. Operating with liquid fuel would assist in rapid diffusion of fuel cell technology into commercial markets, because it will simplify the on-board storage system and use the present infrastructure to supply fuel to passenger cars and commercial

fleets. Compared to H_2/O_2 PEMFCs, the direct alcohol PEMFCs can be more compact without the need of high pressure hydrogen storage or heavy and bulky fuel reformer and can be especially applied to power electric vehicles provided that reasonable performances are achieved.

Liquid fuels, such as low-molecular weight alcohols, with high volumetric and gravimetric energy densities, can be easily handled, stored and transported compared to hydrogen. Among these low-molecular weight alcohols, methanol is at the moment the preferred fuel for low-temperature direct electro-oxidation fuel cells due to a good compromise between reaction kinetics and energy density [2–4]. Particular attention has thus been addressed to the direct methanol fuel cells (DMFCs) in the past decades. However, there are still open questions related to DMFCs such as a serious methanol crossover through the membrane. Another disadvantage of methanol is that it is volatile; moreover, it is relatively toxic. Ethanol has a similar molecular structure of methanol but it is less electrochemically reactive. Ethanol is a green fuel and readily produced from renewable resources. Ethanol is rich of hydrogen and can be used to produce H_2 through reforming process. Ethanol is thus attractive for fuel cells since it can be used directly in direct ethanol fuel cells (DEFCs) or indirectly in H_2/air PEMFCs. The direct ethanol electro-oxidation reaction is reported below:

$$C_2H_5OH + 3\ H_2O \rightarrow 2\ CO_2 + 12\ H^+ + 12\ e^-$$

Complete oxidation of the ethanol molecule involves the release to the anode of twelve electrons.

The electrochemical oxidation of ethanol has been the subject of a large number of recent investigations. In most of previous studies, spectroscopic techniques such as Infrared Spectroscopy (IR), Mass Spectroscopy (MS) and Gas Chromatography (GC) were the most common tools used to identify the products and reaction intermediates of ethanol electro-oxidation. Major products include CO_2, acetaldehyde and acetic acid, but also methane and ethane have been detected [5]. Surface adsorbed CO is still considered as the main intermediate in ethanol electro-oxidation. Additional surface intermediates include other C1 and C2 organic compounds such as ethoxy and acetyl species [5, 6]. It is reported that ethanol electro-oxidation consists of several reaction pathways [7]. Carbon dioxide is the preferred product whereas by-products such as acetaldehyde and acetic acid will cause a decrease of the fuel efficiency. The electro-oxidative removal of CO-like intermediates and the cleavage of C–C bond are the rate-determining steps.

Ethanol electrochemical reaction activity [8] can be enhanced by increasing the reaction temperature or adopting more active electrocatalysts. However, increasing reaction temperature is not, at present, the primary choice because current commercial perfluosulfonic-based polymer electrolyte membranes operating at room pressure dehydrate at high operation temperatures (>100°C), resulting in a high ohmic resistance [9]. It appears clear that ethanol electro-oxidation involves more intermediates and reaction products than methanol [10]. Thus, more active electrocatalysts are needed to promote ethanol electro-oxidation at low temperatures. The nature and structure of the eletrocatalysts play a significant role in the ethanol adsorption and electro-oxidation process. The catalyst preparation procedure affects the catalyst nature and structure, especially the interaction between the different elements forming the active catalyst phase.

In the present work, both binary and ternary carbon-supported Pt-based catalysts have been investigated for ethanol electro-oxidation. These catalysts were prepared according to a simple method

and characterized by X-ray diffraction (XRD) and transmission electron microscope (TEM). Cyclic voltammetry (CV) measurements were used to evaluate the electrocatalytic activities for ethanol electro-oxidation. The aim was to individuate the occurrence of synergistic effects which are relevant to enhance the different reaction steps of the ethanol electro-oxidation process.

2. EXPERIMENTAL DETAILS

Three anode catalysts formulation have been investigated for ethanol oxidation. 50% PtSn/VC (75:25), 50% PtSnIr/VC (75:15:10) and 50% PtSnRh/VC were prepared by chemical reduction with ethylene glycol of metallic precursors, such as $H_2PtCl_6 \cdot 6H_2O$, $SnCl_2 \cdot 2H_2O$, IrCl4·xH2O, $RhCl_3$. The catalysts were prepared by dissolving the metallic precursors in a 75/25 % (v/v) ethylene glycol/H_2O solution (at 70°C), a calculated amount of Carbon Vulcan XC/72R was slowly added to this slurry. This solution was heated at 130°C for two hours under magnetic stirring and subsequently the pH value was adjusted to 13, with NaOH. To favour a complete catalyst reduction process, the temperature was raised to 180°C and maintained for three hours. Afterwards, the slurry was cooled at room temperature and the pH was changed to 7 with H_2SO_4. Finally, the filtered solid was washed with abundant hot water (70 °C) and dried at 80 °C for 12 hours in an oven under N_2 flow. X-Ray diffraction powder (XRD) pattern on the anode catalysts were obtained on a Philips X'Pert X-Ray Diffractometer using a Cu Kα-source. The analysis was made using a Bragg-Brentano para-focusing optical system. The X-Ray diffraction patterns were collected with a scan rate of 0.5°/min. Bulk X-Ray Fluorescence analysis of the catalysts was carried out by a Bruker AXS S4 Explorer Spectrometer. TEM Analysis was carried out by a Philips CM12 Microscope. Electrocatalytic characterization was accomplished by linear potential sweeps and chronoamperometric experiments. The working electrode was a glassy carbon disk (geometric area 0.071 cm^2) covered first by a thin film of catalysts (28 μg loading Pt cm^{-2}) and after then by a thin film of Nafion solution. The counter electrode was a Pt foil of 1 cm^2 of geometric area and the reference electrode was a saturated calomel electrode. The potential was referred to the reversible hydrogen electrode (RHE). The supporting electrolyte was 0.5 M H_2SO_4 and working solutions were essentially a saturated solution of CO in 0.5 M H_2SO_4 or 1 M C_2H_5OH in 0.5 M H_2SO_4. The experiments with ethanol were performed at different temperatures in the 25-60 °C range. The working electrode was preconditioned by cycling for 5 minutes at 0.1 Vs^{-1} between 0.05 and 1.0 V RHE in a 0.5 M H_2SO_4 solution. The active area was determined from the stripping of CO in 0.5 M H_2SO_4. CO was adsorbed at 0.1 V RHE and stripped after proper purging with Ar using 0.01 Vs^{-1} sweep rate [11].

3. RESULTS AND DISCUSSION

3.1 Physico-chemical analysis:

XRF analysis provided information about elemental composition (Table 1).

Table 1. Relative metal concentrations of PtSn/C, PtSnIr/C and PtSnRh/C catalysts from XRF analysis

CATALYST	Pt (% wt)	Sn (% wt)	Ir (% wt)	Rh (% wt)
PtSn/C	75.5	23	-	-
PtSnIr/C	75.07	19.9	4.265	-
PtSnRh/C	76.77	14.8	-	7.87

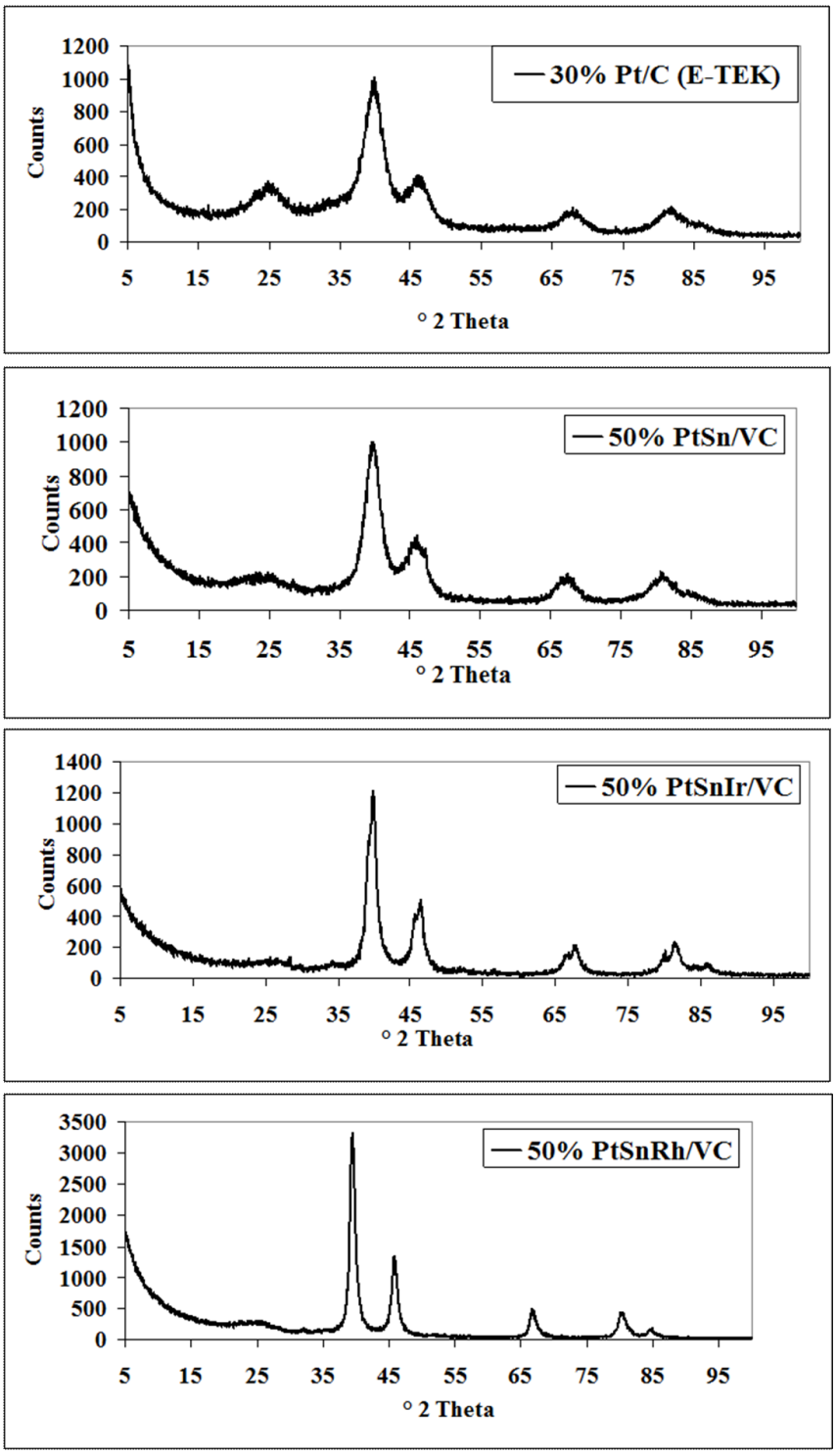

Figure 1. X-Ray diffraction patterns of Pt/C (E-TEK), PtSn/C, PtSnIr/C and PtSnRh/C catalysts.

The Sn content was about 15-20% wt. in the trimetallic catalysts whereas Ir and Rh contents were around 4% - 7 %. XRF results did not converge to 100% metal content due to some matrix effects. XRD patterns of various carbon supported binary and ternary metal catalysts are reported in Fig. 1. The diffraction peak at 20-25° 2 theta observed in all diffraction patterns is attributed to the (002) plane of the exagonal structure of Vulcan XC-72R carbon. All the carbon-supported catalysts synthesized with this method only show a Pt (fcc) crystalline structure.

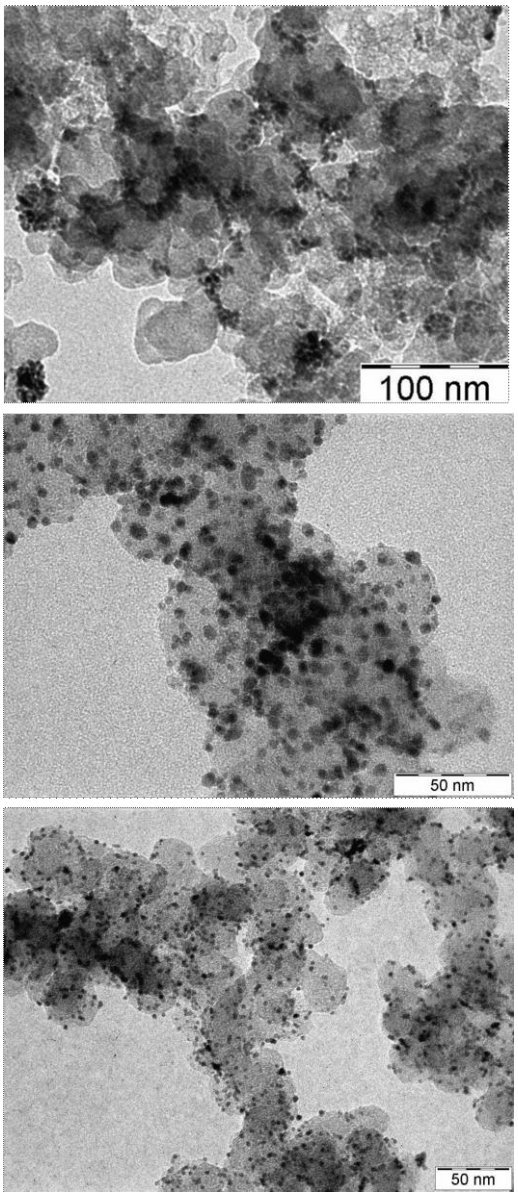

Figure 2. Transmission electron microscopy of PtSn/C, PtSnIr/C and PtSnRh/C catalysts.

The (220) reflections of the Pt-based catalysts were used to calculate the average particle size according to the Sherrer's formula.

$$\tau = \frac{K\lambda}{\beta \cos\theta}$$

where *K* is the shape factor, λ is the x-ray wavelength, β is the line broadening at half the maximum intensity (FWHM) in radians, and θ is the Bragg angle; τ is the mean size of the ordered (crystalline) domains, which may be smaller or equal to the grain size [12-13]. The dimensionless shape factor has a typical value of about 0.9, but it varies with the actual shape of the crystallites. The bimetallic-trimetallic catalysts showed specific differences in the crystallographic properties with respect to a commercial Pt/C catalyst (Table 2). The PtSn/VC had a small crystallite size, 3.2 nm calculated from the (220) reflection broadening [14]. However, this size was slightly larger than a commercial Pt/C catalyst. The crystallite size was about 4.6 nm for PtSnIr/VC and 9 nm for PtSnRh/VC. The lattice parameter of a commercial Pt/C catalyst with cubic fcc structure was 3.9155 Å, whereas it was 3.9329 Å for PtSn/VC, 3.9132 Å for PtSnIr/VC and 3.9668 Å for PtSnRh/VC. The shift of the (220) plane and the difference of lattice parameters indicate that there were interactions between Pt and other metals forming a solid solution.

Table 2. Particle size and lattice parameter of Pt/C, PtSn/C, PtSnIr/C and PtSnRh/C catalysts

CATALYST	Cristallyte size (XRD) nm	Lattice Parameter Å	Particle size (TEM) nm	Surface Area (CO Stripping) m^2/g
Pt/C (E-TEK)	3.0	3.9155	-	-
PtSn/C	3.2	3.9329	3.1	43
PtSnIr/C	4.6	3.9132	4.9	49
PtSnRh/C	9	3.9668	7.9	27

It was observed by TEM, that metal particles of the Pt-based catalysts were fine and reasonably dispersed (Fig. 2). However, for PtSn, despite the fine particle size some degree of agglomeration is observed. The mean particle size of PtSn/C catalysts from TEM was about 3.1 nm with sharp size distribution. Only, the PtSnRh catalyst showed in a few regions large particles that contributed to determine a large average particle size and a relevant discrepancy between TEM and XRD. However, it is pointed out that TEM provides just a local information, whereas the crystallite size determined by XRD is concerning a large amount of sample. From TEM, PtSnIr/VC and PtSnRh/VC had a mean particle size of 4.9 nm and 7.9 nm, respectively. The TEM and XRD results showed that trimetallic nano-sized noble catalysts with high metal loading can be easily prepared by the present method.

3.2 Electrochemical results

Fig. 3 shows the voltammograms of ethanol oxidation for PtSn/VC, PtSnIr/VC and PtSnRh/VC catalysts. Carbon monoxide stripping analysis for the same catalysts is shown in fig. 4. Anodic

polarization curves, in fig. 3obtained at 30 °C, showed that the onset potential for ethanol oxidation occurred at lower potentials for PtSn/VC, but the oxidation reached a maximum at moderate currents. Whereas, the onset potential was progressively higher for PtSnIr/VC and PtSnRh/VC, respectively. The oxidation current density was the highest for PtSnIr/VC. At 60 °C, the oxidation performance was definitively better for PtSnIr and comparable for PtSnRh and PtSn. After holding the potential at 0.65 V RHE for 1 hour, the ethanol oxidation current density for the PtSnIr/C catalyst was the highest among the investigated samples (Fig. 5).

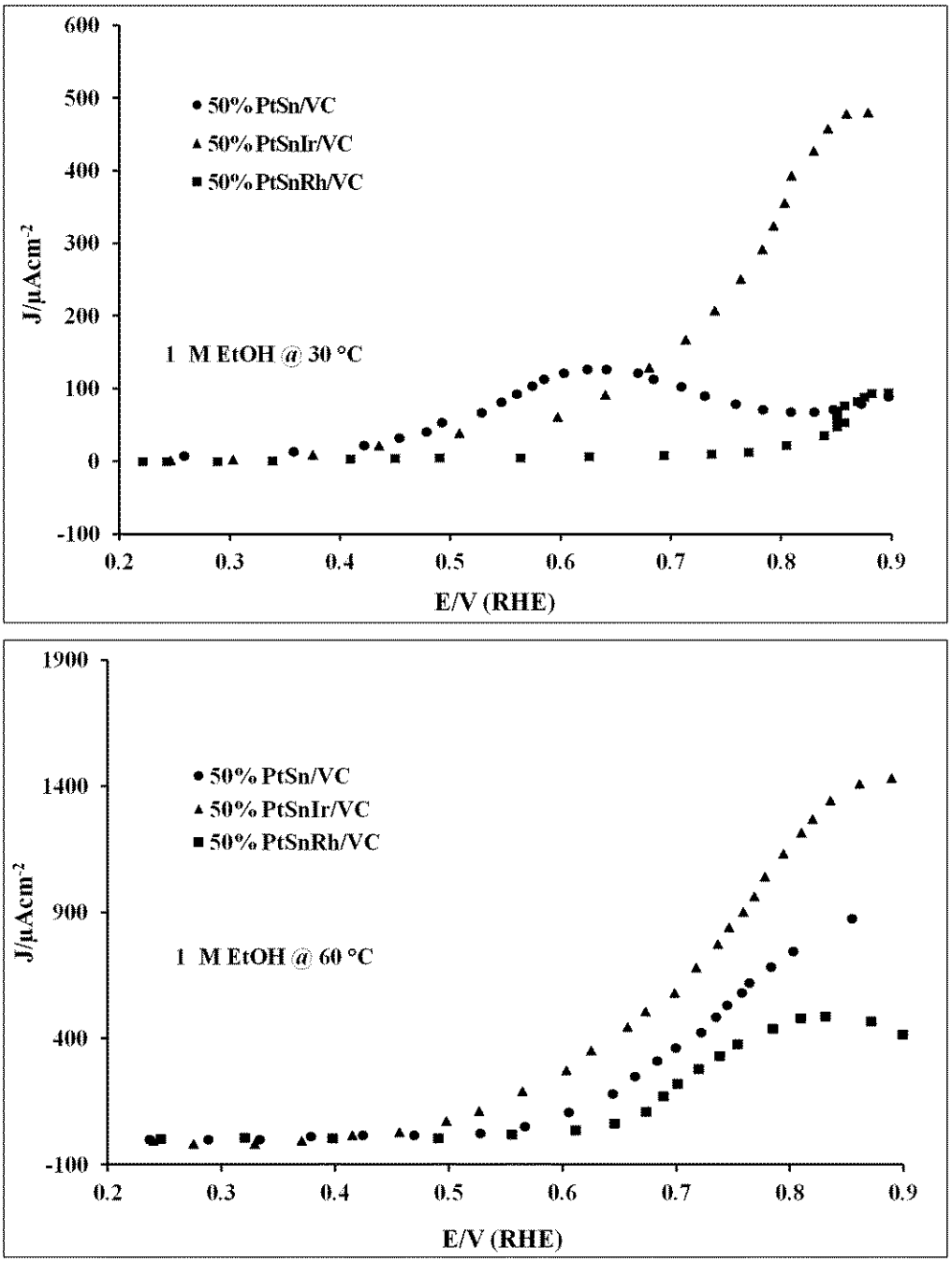

Figure 3. Polarization curves for ethanol oxidation at 30°C and 60°C

At the beginning there was a strong decay of current density, attributed to a progressive poisoning of electrode surface by adsorbed ethanolic residues (CO and CHx). The decay was stronger for the PtSnRh/VC catalyst. This despite several evidences in the literature indicating that Rh atoms possibly help in dissociating $(COCH_3)_{ads}$ species. However, it is pointed out that the PtSnRh/VC catalyst has the largest particle size and the lowest surface area (Table 2). This characteristic may affect coverage properties of ethanolic residues.

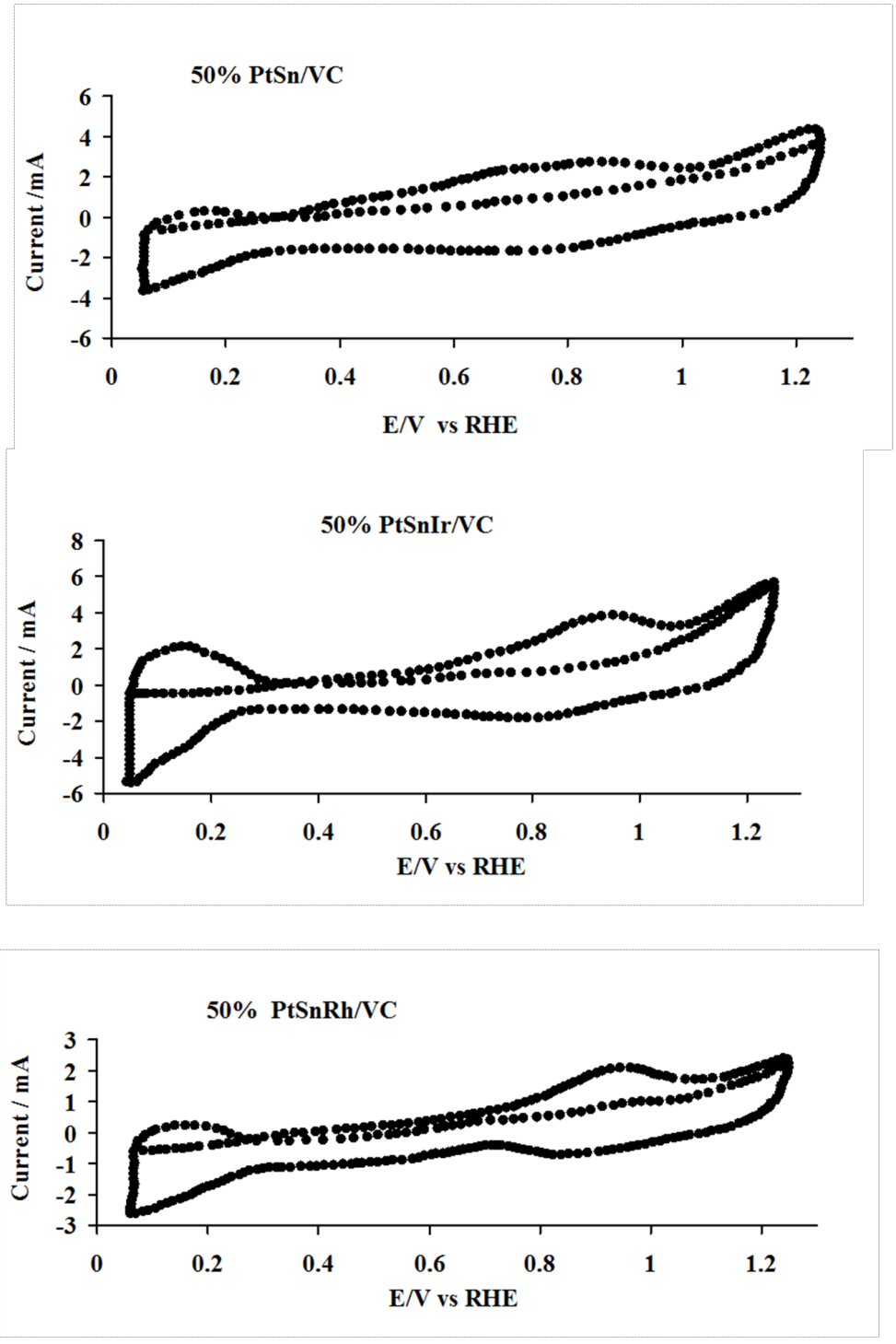

Figure 4. CO Stripping in 0.5 M H_2SO_4 at 0.01 Vs^{-1}

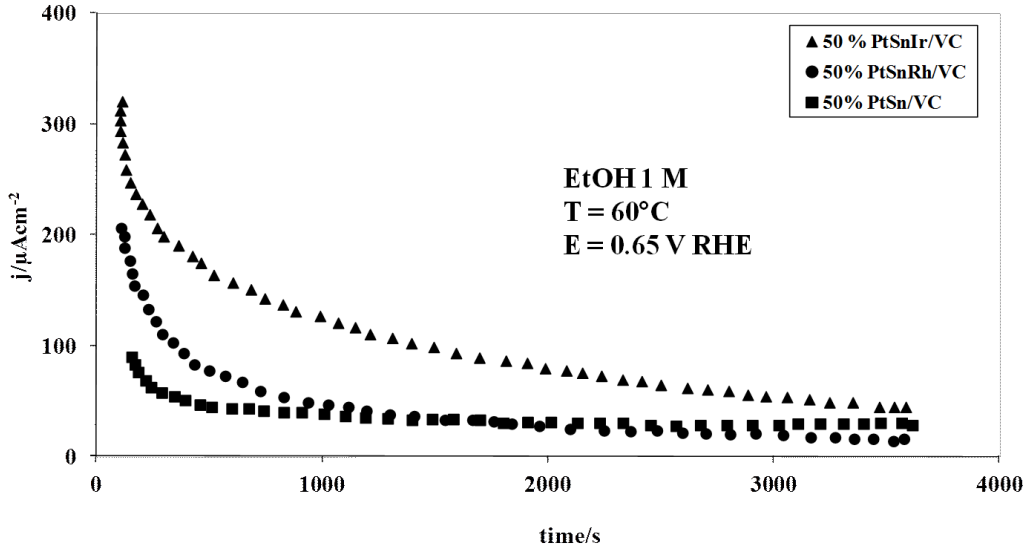

Figure 5. Time study at 60°C and 0.65 V RHE

Also the PtSn catalyst showed moderate oxidation currents despite its small particle size. Thus, it appears that a synergistic effect occurs for the tri-metallic catalysts especially for the PtSnIr. These results also indicate that a strong poisoning caused by the adsorbed intermediates is taking place on PtSnRh/C. It is possible that both Ir and Rh can contribute to the removal of adsorbed species which require another atom of oxygen to achieve total oxidation to CO_2 [15-20]. However, the addition of Ir to the PtSn bimetallic catalyst can result in more easily oxidized species than Rh and this facilitates their removal from the surface.

To distinguish the role of intrinsic activity from that of surface area and to get more insights into the formation of poisoning species, a CO stripping analysis was carried out (Fig. 4). The surface area results are shown in Table 2. The PtSnIr showed the largest surface area despite the fact that its mean particle size was larger than that of PtSn. This result may be due to the larger level at agglomeration in PtSn. The CO stripping curves do not reveal significant shift for CO desorption for the ternary catalysts with respect to the binary catalyst. Thus, the synergism may be due to an enhanced capability of breaking of the C-C bond. This aspect however needs to be confirmed by a proper analysis of the anodic reaction products. Such study will be the objective of a future work.

It is derived that Sn and Ir may be a suitable alternative for ethanol oxidation to Ru or Ru-oxide promoters which are in general more appropriate for methanol oxidation or for oxygen evolution [21-22].

However, proper performances may be achieved only in the presence of a ternary catalyst, such as PtSnIr, where both promoting properties of Sn and Ir are present and possibly a synergetic effect occurs. This requires the use of appropriate preparation procedures to favour the dispersion of metal particles on the support and to achieve a proper degree of alloying in the catalyst. Modification of structure and chemical properties caused by the alloying effect appears relevant to promote ethanol electro-oxidation.

4. CONCLUSION

Pt-Sn based catalysts modified with Ir and Rh have shown syn,ergetic effect for ethanol electro-oxidation. Steady-state ethanol oxidation experiments show larger oxidation currents for the tri-metallic catalysts compared to PtSn. This despite the larger particle size and related lower surface area. However, the catalyst containing Rh showed good initial oxidation current due to the capability to break the C-C bond, but also larger decay with time as a consequence of a significant CO poisoning. TEM and XRD results demonstrate that nano-sized catalysts can be easily synthesized with the present method, in the presence of higher metal loadings.

Structure and particle size characteristics are affected by the catalyst chemistry. The addition of both Sn and Ir to Pt, has a positive effect on the oxidation of ethanol because both metals favour water discharging at lower potentials, than Pt. The role of Pt is to split the C-C bond in the ethanol molecule; this mechanism can be enhanced by Ir and Rh. The catalyst PtSnRh/C, should facilitate the breaking of C-C bond in the ethanol molecule species but it is also affected by a strong coverage of ethanolic residues. This ternary catalyst should be re-evaluated in the presence of a smaller particle size to deconvolute the chemical characteristics from surface area effects. A PtSnIr formulation appears promising and it may be further optimised in terms of relative atomic ratios.

ACKNOWLEDGEMENTS
The authors thank National Council of the Research (CNR) and INIFTA for the "Short Term Mobility Programme 2010" between Italy and Argentina.

References

1. B.D. McNicol, D.A.J. Rand, K.R. Williams, *J. Power Sources*, 83 (1999) 15
2. H. Dohle, H. Schmitz, T. Bewer, et al., *J. Power Sources*, 106 (2002) 313
3. X.M. Ren, P. Zelenay, S. Thomas, et al., *J. Power SourceS*, 86 (2000) 111
4. S.C. Thomas, X.M. Ren, S. Gottsfeld, et al., *Electrochim. Acta*, 47 (2002) 3741
5. T. Iwasita, E. Pastor, *Electrochim. Acta*, 39 (1994) 531
6. B. Beden, M.-C. Morin, F. Hahn, et al., *J. Electroanal. Chem.*, 229 (1987) 353
7. C. Lamy, E.M. Belgsir, J.-M. Léger, *J. Appl. Electrochem.*, 31 (2001) 799
8. A.S. Aricò, P. Cretì, P.L. Antonucci, V. Antonucci, *Electrochem .Solid State Lett.*, (1998) 1 (2) , pp. 66-68
9. C. Yang, S. Srinivasan, A.S. Arico, P. Creti, et al., *Electrochem. Solid State Lett.*, 4 (2001) A31
10. S.C. Zignani, V. Baglio, J. Linares, G. Monforte, E.R. Gonzalez, A.S. Aricò, *Electrochimica Acta*, 70, (2012) 255-265
11. A.S. Aricò, V. Baglio, A. Di Blasi, E. Modica, G. Monforte, V. Antonucci, *Journal of Electroanalytical Chemistry*, 576 (1) , (2005) 161-169
12. P. Scherrer, *Göttinger Nachrichten Gesell.*, 2, (1918) 98
13. A. Patterson, A. "The Scherrer Formula for X-Ray Particle Size Determination". *Phys. Rev.* 56 (10), (1939) 978–982
14. S.C. Zignani, E.R. Gonzalez, V. Baglio, S. Siracusano, A.S. Aricò, *Int. J. Electrochem. Sci.*, 7 (2012) 3155-3166
15. B. Pierozynski, *Int. J. Electrochem. Sci.*, 7 (2012) 4488-4497
16. B. Pierozynski, *Int. J. Electrochem. Sci.*, 7 (2012) 4261-4271

17. B.-J. Su, K-W. Wang, C.-J. Tseng, C.-H. Wang, Y.-J. Hsueh, *Int. J. Electrochem. Sci.*, 7 (2012) 5246-5255
18. A. Tabet-Aoul, F. Saidani, D. Rochefort, M. Mohamedi, *Int. J. Electrochem. Sci.*, 6 (2011) 6385-6397
19. H.D. Herrera-Mendez, P.Roquero, M.A. Smit, L.C. Ordonez, *Int. J. Electrochem. Sci.*, 6 (2011) 4454-4469
20. H. Li, D. Kang, H. Wang, R. Wang, *Int. J. Electrochem. Sci.*, 6 (2011) 1058-1065
21. J. C. Cruz, V. Baglio, S. Siracusano, V. Antonucci, A. S. Aricò, R. Ornelas, L. Ortiz-Frade, G. Osorio-Monreal, S. M. Duron-Torres, L. G. Arriaga, *Int. J. Electrochem. Sci.*, 6 (2011) 6607-6619
22. V. Baglio, A. Di Blasi, E. Modica, P. Cretì, V. Antonucci, A. S. Aricò, *Int. J. Electrochem. Sci.*, 1 (2006) 71-79